ANALYSIS OF CRACKED PLATES BY A RITZ TYPE APPROACH

Bruno Henrique de Sena e Oliveira

bhsena@gmail.com

EMBRAER S.A.

12227-901, São José dos Campos, SP, Brazil

Eliseu Lucena Neto

Francisco Alex Correia Monteiro

eliseu@ita.br

facm@ita.br

Instituto Tecnológico de Aeronáutica

12228-900, São José dos Campos, SP, Brazil

Abstract. *The present paper deals with the analysis of the stress intensity factors of cracked plates using the Ritz method. This type of analysis is essential for the design of wing and fuselage skins in aerospace engineering. A set of hierarchic polynomials is used to define the displacement approximations of the cracked plate. The plate is divided into a number of panels and treated as an assembly of them so that the discontinuity associated with cracks may be taken into account. Examples illustrate the h- and p-convergence of the proposed approach, comparing its accuracy and efficiency with those of finite element models in predicting stress intensity factors.*

Keywords: *Cracked plate, Ritz method, Hierarchic set, Polynomial set, Stress intensity factor*

1 INTRODUCTION

Stiffened panels are widely used in aerospace, naval and mechanical structures whenever weight is an important concern. The occurrence of cracks, which are among the most common defects that happen in mechanical components, is inevitable, and since cracks are associated with singularities in the stress field, the design of plates in the presence of cracks requires extensive knowledge of the stress distribution.

The strength of a cracked plate is measured by the stress intensity factor which determines the rate of the crack growth in cyclic loading. Each plate and loading configuration will lead to a different stress intensity factor, and will require either a very detailed analytic solution or a finite element model with many degrees of freedom, given the complexity of the stress field, even for simple geometries. Because of such laboriousness, there are some works devoted to collect as many stress intensity factors as possible (Rooke & Cartwright, 1976; Tada et al., 2000), but even small design modifications can lead to great changes in the crack behavior. Many of the results from these compendiums were obtained using analytic approaches (Isida et al., 1973; Poe, 1971) but sophisticated numerical procedures have been developed and applied to the determination of stress intensity factors in many contexts (Fawaz & Andersson, 2004; Andersson et al., 1995). The *p*-refinement of finite element method is usually associated with these procedures.

Some special Ritz schemes, on the other hand, have been used in many applications related to vibrations and buckling of plates (Bardell, 1991; Beslin & Nicolas, 1996) and cracked panels (Barrete et al., 2000; Kumar & Paik, 2004; Brighenti, 2005). Our approach developed herein is another special form of the Ritz method for which the bases are constructed from a hierarchic polynomial set, with the two first elements being the linear Lagrange polynomials and the remaining ones constructed from a single integration of Legendre polynomials. A hierarchic set has the characteristic that a generated basis includes all bases of lesser orders. A major advantage in adopting this type of set is the possibility of performing all matrix integrations just once by choosing a sufficient large order. In this way, only one significant computational expense is ever incurred.

There have been programs that made use of pre-computed integrals (Basu et al., 1977) and of the same hierarchic set of our model (Babuska et al., 1989)., but these refinements, and *p*-refinements in general, are limited by the numerical stability of the integrals. We will push the use of the hierarchic set to as high as 50 functions using symbolic integration. We will then introduce a simple method of uniting various Ritz subdomains and create a simple and flexible approach for accurate stress intensity factor predictions of finite plates.

2 FUNDAMENTALS

In our formulations we consider plates with in-plane displacements, under plane stress condition, behaving as a membrane.

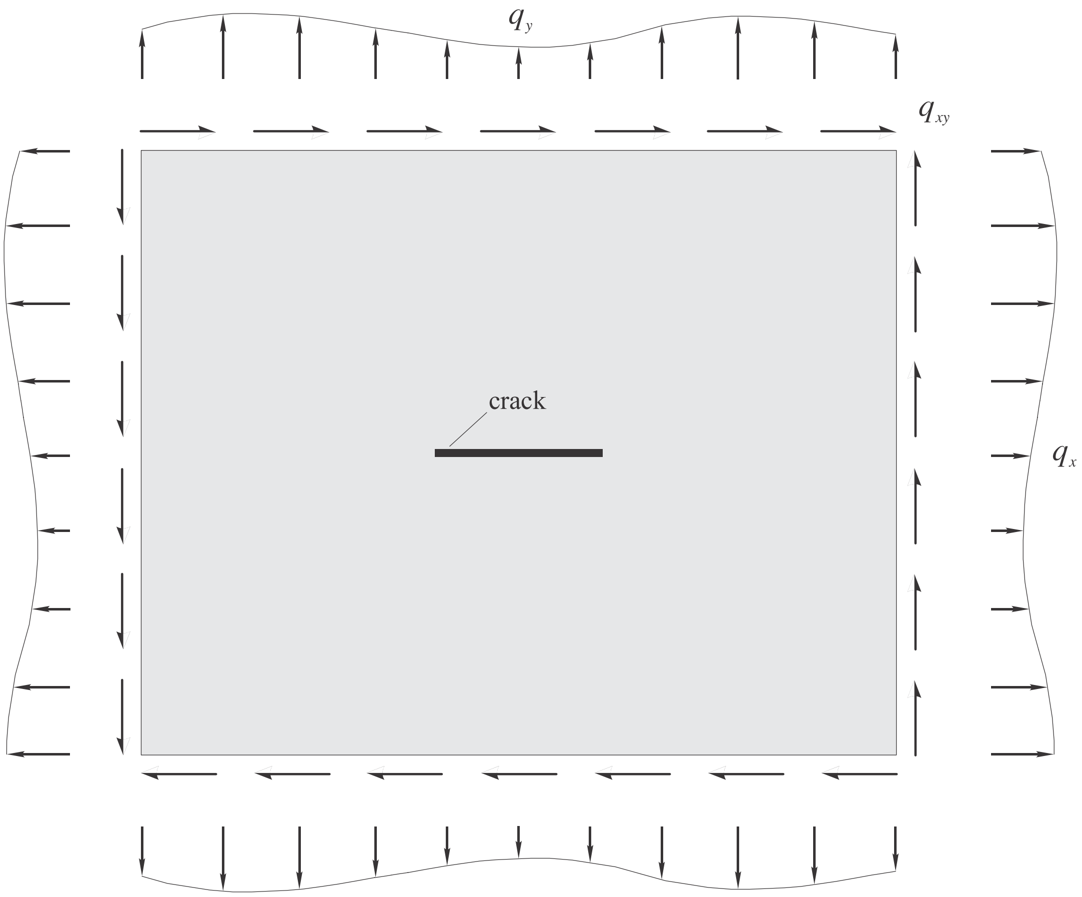

Figure 1: Cracked plate

2.1 Potential energy

We consider the cracked plate of Fig. 1, under the distributed loads q_x,q_y and q_{xy} applied to the edges. The plate is divided into several panels (see Fig. 2a), with edges delimited by cracks, lines of continuity or the plate edges. An isolated panel is shown in Fig. 2b.

Each panel has side lengths a_i, b_i and thickness h. Assuming membrane deformations, the strain energy of a panel i reads

$$U_{pi} = \frac{1}{2}\int_0^{b_i}\int_0^{\mathrm{a_i}} \boldsymbol{\epsilon}_\mathrm{m}^\mathrm{T}\ \mathbf{A}\ \boldsymbol{\epsilon}_\mathrm{m} dxdy \tag{1}$$

where $\boldsymbol{\epsilon}_m = \lfloor u_{,x} \quad v_{,y} \quad u_{,y} + v_{,x} \rfloor^T$ and **A** is the membrane rigidity.

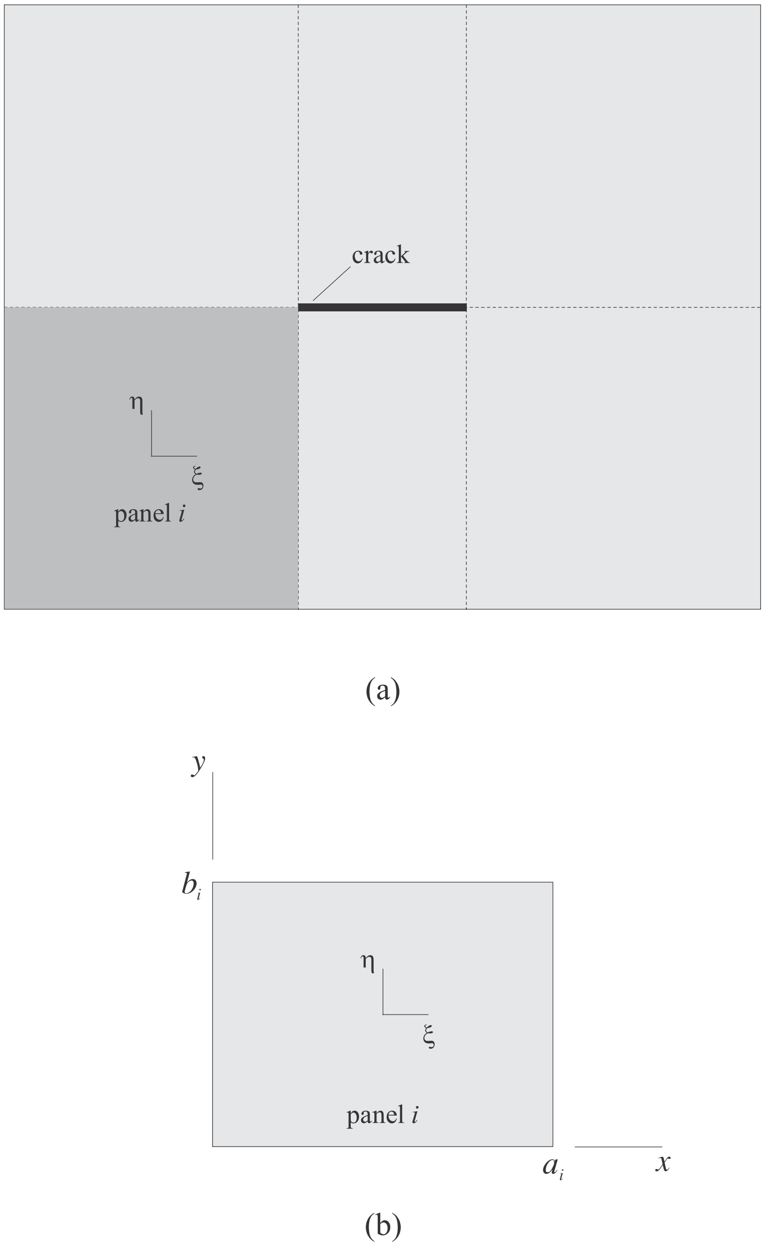

Figure 2: (a) Plate divided into six panels; (b) isolated panel

The potential energy of the applied loads is given by

$$V_i = -\int_0^{a_i}\left[\left(q_y v + q_{xy} u\right)_{y=b_i} - \left(q_y v + q_{xy} u\right)_{y=0}\right] dx$$
$$- \int_0^{b_i}\left[\left(q_x u + q_{xy} v\right)_{x=a_i} - \left(q_x u + q_{xy} v\right)_{x=0}\right] dy \qquad (2)$$

The loading applied to an edge of the plate is not necessarily equal to the loading applied to the opposite edge, but it is denoted by the same symbol in the above equation for simplicity.

The potential energy of the entire plate will be

$$\Pi = \sum \left(U_{pi} + V_i \right) \tag{3}$$

if the displacements $u(x, y)$ and $v(x, y)$ are continuous between panels (except for crack locations). Therefore we will need to impose continuity C^0 in all panel junctions.

2.2 Discretization of the potential energy

Let ξ and η be nondimensional coordinates defined in the domain of each panel by

$$\xi = \frac{2}{a_i} x - 1 \qquad \eta = \frac{2}{b_i} y - 1 \tag{4}$$

where $-1 \leq \xi \leq 1$ and $-1 \leq \eta \leq 1$ as shown in Fig. 2. We will then impose the following approximation to the local panel displacements

$$u = \sum \alpha_j G_j(\xi, \eta) = \boldsymbol{\alpha}^T \mathbf{G} \qquad v = \sum \beta_j H_j(\xi, \eta) = \boldsymbol{\beta}^T \mathbf{H} \tag{5}$$

with $G_j(\xi, \eta)$, $H_j(\xi, \eta)$ being linearly independent functions and α_j, β_j unknown coefficients. Substitution of Eq. (5) into Eq. (1) reads

$$\begin{aligned} U_{pi} &= \frac{1}{4} \int_{-1}^{1} \int_{-1}^{1} \begin{Bmatrix} \boldsymbol{\alpha} \\ \boldsymbol{\beta} \end{Bmatrix}^T \begin{bmatrix} b_i \mathbf{G}_{,\xi}^T & \mathbf{0}^T \\ \mathbf{0}^T & a_i \mathbf{H}_{,\eta}^T \\ a_i \mathbf{G}_{,\eta}^T & b_i \mathbf{H}_{,\xi}^T \end{bmatrix}^T \mathbf{A} \begin{bmatrix} b_i \mathbf{G}_{,\xi}^T & \mathbf{0}^T \\ \mathbf{0}^T & a_i \mathbf{H}_{,\eta}^T \\ a_i \mathbf{G}_{,\eta}^T & b_i \mathbf{H}_{,\xi}^T \end{bmatrix} \begin{Bmatrix} \boldsymbol{\alpha} \\ \boldsymbol{\beta} \end{Bmatrix} d\xi d\eta \\ &= \frac{1}{2} \mathbf{c}_i^T \mathbf{k}_p \mathbf{c}_i \end{aligned} \tag{6}$$

where

$$\mathbf{c}_i = \begin{Bmatrix} \boldsymbol{\alpha} \\ \boldsymbol{\beta} \end{Bmatrix} \tag{7}$$

and

$$\mathbf{k}_p = \frac{1}{2}\begin{bmatrix} \int_{-1}^{1}\int_{-1}^{1} \mathbf{N}_u^T\, \mathbf{A}\, \mathbf{N}_u d\xi d\eta & \int_{-1}^{1}\int_{-1}^{1} \mathbf{N}_u^T\, \mathbf{A}\, \mathbf{N}_v d\xi d\eta \\ \text{sym.} & \int_{-1}^{1}\int_{-1}^{1} \mathbf{N}_v^T\, \mathbf{A}\, \mathbf{N}_v d\xi d\eta \end{bmatrix} \quad \mathbf{N}_u = \begin{bmatrix} b_i \mathbf{G}_{,\xi}^T \\ \mathbf{0}^T \\ a_i \mathbf{G}_{,\eta}^T \end{bmatrix} \quad \boldsymbol{N}_v = \begin{bmatrix} \mathbf{0}^T \\ a_i \mathbf{H}_{,\eta}^T \\ b_i \mathbf{H}_{,\xi}^T \end{bmatrix}. \quad (8)$$

Substitution of Eq. (5) into Eq. (2) yields

$$\begin{aligned} V_i &= -\frac{a_i}{2}\int_{-1}^{1}\left(\begin{Bmatrix}\boldsymbol{\alpha}\\ \boldsymbol{\beta}\end{Bmatrix}^T \begin{Bmatrix} q_{xy}\mathbf{G} \\ q_y \mathbf{H}\end{Bmatrix}_{\eta=1} - \begin{Bmatrix}\boldsymbol{\alpha}\\ \boldsymbol{\beta}\end{Bmatrix}^T \begin{Bmatrix} q_{xy}\mathbf{G} \\ q_y \mathbf{H}\end{Bmatrix}_{\eta=-1}\right) d\xi \\ &\quad -\frac{b_i}{2}\int_{-1}^{1}\left(\begin{Bmatrix}\boldsymbol{\alpha}\\ \boldsymbol{\beta}\end{Bmatrix}^T \begin{Bmatrix} q_x\mathbf{G} \\ q_{xy} \mathbf{H}\end{Bmatrix}_{\xi=1} - \begin{Bmatrix}\boldsymbol{\alpha}\\ \boldsymbol{\beta}\end{Bmatrix}^T \begin{Bmatrix} q_x\mathbf{G} \\ q_{xy} \mathbf{H}\end{Bmatrix}_{\xi=-1}\right) d\eta \\ &= -\mathbf{c}_i^T \mathbf{f}_i \end{aligned} \quad (9)$$

with

$$\mathbf{f}_i = \frac{a_i}{2}\int_{-1}^{1}\begin{Bmatrix} q_{xy}\mathbf{G} \\ q_y \mathbf{H}\end{Bmatrix}_{\eta=-1}^{\eta=1} d\xi + \frac{a_i}{2}\int_{-1}^{1}\begin{Bmatrix} q_x\mathbf{G} \\ q_{xy} \mathbf{H}\end{Bmatrix}_{\xi=-1}^{\xi=1} d\eta. \quad (10)$$

Finally, we substitute Eqs. (6), (9) into Eq. (3) to obtain the discrete plate potential energy

$$\begin{aligned} \Pi &= \sum \mathbf{c}_i^T \left(\frac{1}{2}\mathbf{k}_i\, \mathbf{c}_i - \mathbf{f}_i\right) \\ &= \mathbf{C}^T \left(\frac{1}{2}\mathbf{K}\, \mathbf{C} - \mathbf{F}\right). \end{aligned} \quad (11)$$

The stiffness matrix of the entire plate **K**, the vector of applied forces **F** and the coefficients vector **C** are given by

$$\mathbf{K} = \begin{bmatrix} \mathbf{k}_1 & \mathbf{0} & \cdots \\ \mathbf{0} & \mathbf{k}_2 & \cdots \\ \vdots & \vdots & \ddots \end{bmatrix} \qquad \mathbf{F} = \begin{Bmatrix} \mathbf{f}_1 \\ \mathbf{f}_2 \\ \vdots \end{Bmatrix} \qquad \mathbf{C} = \begin{Bmatrix} \mathbf{c}_1 \\ \mathbf{c}_2 \\ \vdots \end{Bmatrix}. \quad (12)$$

2.3 Continuity across the panel interfaces

For the approximation described in Eq. (5) we will use, both for u and v, a set of C^0 hierarchic polynomials derived from Legendre orthogonal polynomials and given by, in the form proposed by Zhu (1985)

$$\phi_r(\lambda) = \sum_{n=0}^{r/2} \frac{(-1)^n(2r-2n-5)!!}{2^n n!(r-2n-1)!} \lambda^{r-2n-1} \qquad r > 2. \tag{13}$$

Here λ may be either ξ or η, $r!! = r(r-2)\cdots(2 \text{ or } 1), 0!! = (-1)!! = 1$ and $r/2$ denotes its own integer part. The functions Eq. (13) will always be zero in the ends $\lambda = \pm 1$. Therefore these functions will only contribute to the internal displacements of the panel, and we can choose the first two functions of the set as being

$$\phi_1(\lambda) = \frac{1}{2} + \frac{1}{2}\lambda, \qquad \phi_2(\lambda) = \frac{1}{2} - \frac{1}{2}\lambda. \tag{14}$$

Since they are the only functions that are nonzero at $\lambda = \pm 1$, we will work with them to determine boundary conditions and continuity between panels.

We write **G** and **H** given in Eq. (5) in the form

$$\mathbf{G} = \begin{Bmatrix} \phi_1(\xi)\mathbf{\Phi}_{g\eta} \\ \phi_2(\xi)\mathbf{\Phi}_{g\eta} \\ \vdots \\ \phi_p(\xi)\mathbf{\Phi}_{g\eta} \end{Bmatrix}_{pq\times 1} \qquad \mathbf{H} = \begin{Bmatrix} \phi_1(\xi)\mathbf{\Phi}_{h\eta} \\ \phi_2(\xi)\mathbf{\Phi}_{h\eta} \\ \vdots \\ \phi_r(\xi)\mathbf{\Phi}_{h\eta} \end{Bmatrix}_{rs\times 1} \tag{15}$$

so that

$$\mathbf{\Phi}_{g\eta} = \lfloor \phi_1(\eta) \quad \phi_2(\eta) \quad \cdots \quad \phi_q(\eta) \rfloor^T \qquad \mathbf{\Phi}_{h\eta} = \lfloor \phi_1(\eta) \quad \phi_2(\eta) \quad \cdots \quad \phi_s(\eta) \rfloor^T. \tag{16}$$

The indexes p, q, r, s are the number of functions chosen in each direction for each displacement field (note that they must always be greater than 1).

Here we make use of an operator called Kronecker product (Abadir & Magnus, 2005), defined as the product of two matrices

$$\mathbf{P}\otimes\mathbf{Q} = \begin{bmatrix} p_{11}\mathbf{Q} & p_{12}\mathbf{Q} & \cdots \\ p_{21}\mathbf{Q} & p_{22}\mathbf{Q} & \cdots \\ \vdots & \vdots & \ddots \end{bmatrix} \tag{17}$$

where p_{ij} are elements of $\mathbf{P}$. If

$$\boldsymbol{\Phi}_{g\xi} = \lfloor \phi_1(\xi) \quad \phi_2(\xi) \quad \cdots \quad \phi_q(\xi) \rfloor^T \qquad \boldsymbol{\Phi}_{h\xi} = \lfloor \phi_1(\xi) \quad \phi_2(\xi) \quad \cdots \quad \phi_s(\xi) \rfloor^T, \tag{18}$$

we simply write

$$\mathbf{G} = \boldsymbol{\Phi}_{g\xi} \otimes \boldsymbol{\Phi}_{g\eta} \qquad \mathbf{H} = \boldsymbol{\Phi}_{h\xi} \otimes \boldsymbol{\Phi}_{h\eta}. \tag{19}$$

The application of the boundary conditions is pretty straightforward, as listed in Table 1. Basically each coefficient in Eq. (5) is associated with one of the products of functions in the sets of Eq. (19). All the coefficients associated with the first two functions of the set, described in Eq. (14), control the displacement of one edge of the panel. For instance, a panel with null edge displacements would have all of the coefficients associated with the functions listed in Table 1 set to zero.

Table 1: Functions with coefficients to be set to zero in order to satisfy the geometric boundary conditions

Constrained edge	$\phi_1(\xi)$	$\phi_2(\xi)$	$\phi_1(\eta)$	$\phi_2(\eta)$
top			X	
bottom				X
left		X		
right	X			

In order to impose continuity between panels we will determine, as an example, a continuous displacement between one panel i and one panel $i+1$ on its right:

$$u^i(1,\eta) = u^{i+1}(-1,\eta). \tag{20}$$

Using Eq. (5) and Eq. (20) we write

$$\{\alpha^i\}^T \left(\boldsymbol{\Phi}_{g\xi} \otimes \boldsymbol{\Phi}_{g\eta}\right)_{(1,\eta)} = \{\alpha^{i+1}\}^T \left(\boldsymbol{\Phi}_{h\xi} \otimes \boldsymbol{\Phi}_{h\eta}\right)_{(-1,\eta)}. \tag{21}$$

At the interface, all the hierarchic functions in the ξ direction will be zero, leaving only one of the two first functions Eq. (14):

$$\mathbf{\Phi}_{g\xi}(1) = \lfloor 0 \quad 1 \quad 0 \quad \cdots \quad 0 \rfloor^T \qquad \mathbf{\Phi}_{g\xi}(-1) = \lfloor 1 \quad 0 \quad 0 \quad \cdots \quad 0 \rfloor^T. \tag{22}$$

If we apply Eq. (22) to Eq. (21),

$$\sum_{j=1}^{q} \alpha_{q+j}^{i} \phi_j(\eta) = \sum_{j=1}^{q} \alpha_j^{i+1} \phi_j(\eta). \tag{23}$$

Since we are using the same linearly independent functions ϕ_j in both panels, Eq. (23) implies

$$\alpha_{q+j}^{i} = \alpha_j^{i+1} \qquad j = 1,2,\dots,q. \tag{24}$$

Every continuity condition will then produce an equality constraint such as Eq. (24), between two or more coefficients. The original number of independent coefficients will be reduced. For m independent coefficients, we propose a $\mathbf{T}$ matrix, composed only of ones and zeroes, to relate such coefficients to the k total coefficients according to Eq. (24):

$$\mathbf{C} = \mathbf{T}_{k\times m}\,\bar{\mathbf{C}}. \tag{25}$$

In this matrix we can also impose the boundary conditions, by setting any coefficient j we want to zero simply by letting the j-th column of $\mathbf{T}$ entirely equal to zero.

Substituting Eq. (25) into Eq. (11), the potential energy becomes

$$\Pi = (\mathbf{T}\,\bar{\mathbf{C}})^T \left(\frac{1}{2}\mathbf{K}\,\mathbf{T}\,\bar{\mathbf{C}} - \mathbf{F}\right) = \bar{\mathbf{C}}^T \left(\frac{1}{2}\bar{\mathbf{K}}\,\bar{\mathbf{C}} - \bar{\mathbf{F}}\right) \tag{26}$$

where

$$\bar{\mathbf{K}} = \mathbf{T}^{\mathrm{T}}\mathbf{K}\,\mathbf{T} \qquad \bar{\mathbf{F}} = \mathbf{T}^{\mathrm{T}}\mathbf{F} \tag{27}$$

are the stiffness matrix and force vector associated to the independent coefficients. Finally the problem is described by the stationary point of Π in relation to $\bar{\mathbf{C}}$:

$$\frac{\partial \Pi}{\partial \bar{\mathbf{C}}} = 0 \qquad \bar{\mathbf{K}}\,\bar{\mathbf{C}} = \bar{\mathbf{F}}. \tag{28}$$

Proceedings of the XXXVIII Iberian Latin-American Congress on Computational Methods in Engineering
P.O. Faria, R.H. Lopez, L.F.F. Miguel, W.J.S. Gomes, M. Noronha (Editores), ABMEC, Florianópolis, SC, Brazil, November 5-8, 2017.

2.4 Precomputing of integrals

In the evaluation of the force vector, it is simple to precompute the integrals (10) for a given type of load (linear, parabolic, …). We limit ourselves to the constant and parabolic loadings, and the use of the same functions for $\mathbf{G}$ and $\mathbf{H}$ in the ξ and η directions. For instance, a constant load q_y would give

$$\mathbf{f}_{q_y} = \frac{a_i}{2}\int_{-1}^{1}\{q_y\mathbf{H}\}_{\eta=-1}^{\eta=1} d\xi. \tag{29}$$

Using Eq. (19),

$$\mathbf{f}_{q_y} = \frac{a_i q_y}{2}\int_{-1}^{1}\{\mathbf{\Phi}_{\mathrm{h}\xi}\otimes\mathbf{\Phi}_{h\eta}\}_{\eta=-1}^{\eta=1} d\xi = \frac{a_i q_y}{2}\int_{-1}^{1}\mathbf{\Phi}_{\mathrm{h}\xi}\, d\xi\otimes\{\mathbf{\Phi}_{h\eta}^{T}\}_{\eta=-1}^{\eta=1}. \tag{30}$$

A precomputed vector would be simply

$$\int_{-1}^{1}\mathbf{\Phi}_{h\xi}\, d\xi. \tag{31}$$

It is easy to see that if we compute this vector with the highest possible number of functions in our model, the vector could be reused for lower refinement by excluding from the set the exceeding elements. The above precomputation approach can be extended in the evaluation of the stiffness matrix. For instance, suppose we want to precompute the integral

$$\int_{-1}^{1}\int_{-1}^{1}\mathbf{N}_u^T\,\mathbf{A}\,\mathbf{N}_{\mathrm{v}}\, d\xi d\eta \tag{32}$$

given in Eq. (8). In order to carry out with the integration, we define the vectorization operation which converts a matrix to a column vector (Abadir & Magnus, 2005). So the vectorization of a $m \times n$ matrix $\mathbf{P}$ is

$$\mathrm{vec}(\mathbf{P}) = \lfloor p_{11} \quad p_{21} \quad \cdots \quad p_{12} \quad p_{22} \quad \cdots \quad p_{1n} \quad p_{2n} \quad \cdots\rfloor^T. \tag{33}$$

This operator and the Kronecker product defined in Eq. (17) have the following useful property between three matrices $\mathbf{P}$, $\mathbf{Q}$ and $\mathbf{R}$:

$$\mathrm{vec}(\mathbf{P}\,\mathbf{Q}\,\mathbf{R}) = (\mathbf{R}^T\otimes\mathbf{P})\mathrm{vec}(\mathbf{Q}). \tag{34}$$

Applying property Eq. (34) to Eq. (32) gives

$$\mathrm{vec}\left(\int_{-1}^{1}\int_{-1}^{1}\mathbf{N}_u^T\,\mathbf{A}\,\mathbf{N}_v\, d\xi d\eta\right) = \int_{-1}^{1}\int_{-1}^{1}\mathbf{N}_v^T\otimes\mathbf{N}_u^T\, d\xi d\eta\ \mathrm{vec}(\mathbf{A}). \tag{35}$$

Proceedings of the XXXVIII Iberian Latin-American Congress on Computational Methods in Engineering
P.O. Faria, R.H. Lopez, L.F.F. Miguel, W.J.S. Gomes, M. Noronha (Editores), ABMEC, Florianópolis, SC, Brazil, November 5-8, 2017.

Using Eq. (19), the Kronecker product leads to several integrals of the shape functions. For instance,

$$\int_{-1}^{1}\int_{-1}^{1} a_i \mathbf{H}_{,\eta}^T \otimes b_i \mathbf{G}_{,\xi}^T \, d\xi d\eta = b_i a_i \int_{-1}^{1}\int_{-1}^{1} \left(\mathbf{\Phi}_{h\xi} \otimes \mathbf{\Phi}_{h\eta,\eta}\right)^T \otimes \left(\mathbf{\Phi}_{g\xi,\xi} \otimes \mathbf{\Phi}_{g\eta}\right)^T \, d\xi d\eta. \quad (36)$$

It is a simple matter of programming to reduce the integration problem to three standard matrices:

$$\int_{-1}^{1} \mathbf{\Phi}_{h\xi} \, \mathbf{\Phi}_{h\xi}^T d\xi \qquad \int_{-1}^{1} \mathbf{\Phi}_{h\xi,\xi} \, \mathbf{\Phi}_{h\xi}^T d\xi \qquad \int_{-1}^{1} \mathbf{\Phi}_{h\xi,\xi} \, \mathbf{\Phi}_{h\xi,\xi}^T d\xi. \quad (37)$$

Once again, if we compute these matrices with the highest possible number of functions in our model, they could be reused for lower refinement by excluding from the set the exceeding elements.

3 NUMERICAL TESTS

The performance of the proposed Ritz scheme will be illustrated next by means of three examples. The first plate under uniaxial parabolic will illustrate the capabilities of p-refinement when dealing with simple problems and two cracked plates will show how the proposed model behaves in the presence of the singularity.

3.1 Plate under uniaxial parabolic load

The case of a simple plate under uniaxial parabolic load is shown in Fig. 3. For our numerical solution we used $a = 1,\ q_0 = 1,\ E = 1$, thickness $h = 1$ and $\nu = 0.3$ (consistent units). Due to symmetry, only the top right quarter of the plate is modeled. The geometric boundary conditions

$$u = 0 \quad \text{at} \quad x = 0 \qquad v = 0 \quad \text{at} \quad y = 0 \quad (38)$$

must be imposed. Table 2 compares our results with benchmarks found in Cowper et al. (1970). A single panel (1×1 mesh) with crescent p (number of functions in each ξ and η directions used in each displacement field) is employed, and the results for displacement in point C and membrane forces at point A are shown. Excellent agreement is observed for $p = 9$. The effect of h- and p-refinement in the convergence of the displacement u at point C is depicted in Fig.4.

Proceedings of the XXXVIII Iberian Latin-American Congress on Computational Methods in Engineering
P.O. Faria, R.H. Lopez, L.F.F. Miguel, W.J.S. Gomes, M. Noronha (Editores), ABMEC, Florianópolis, SC, Brazil, November 5-8, 2017.

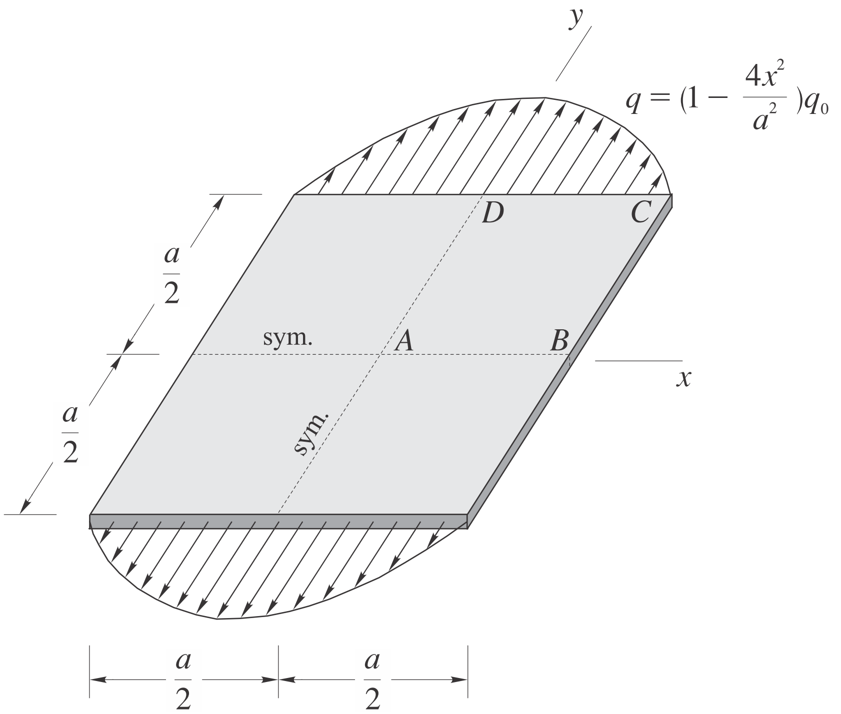

Figure 3: Plate under uniaxial parabolic load

Table 2: Plate under uniaxial parabolic load (1 × 1 mesh)

p	$\frac{100Ehu_c}{(1-\nu^2)q_0a}$	$\frac{10Ehv_c}{(1-\nu^2)q_0a}$	$\frac{N_{x_A}}{q_0}$	$\frac{N_{y_A}}{q_0}$	$\frac{N_{xy_A}}{q_0}$
2	-5.353	2.375	-0.035	0.891	0.000
3	1.995	1.338	-0.150	0.884	0.000
4	1.877	1.287	-0.178	0.822	0.000
5	1.795	1.278	-0.136	0.864	0.000
8	1.783	1.277	-0.141	0.859	0.000
9	1.784	1.277	-0.141	0.859	0.000
	1.784†	1.277†	-0.141†	0.859†	0.000

† Cowper et al. (1970)

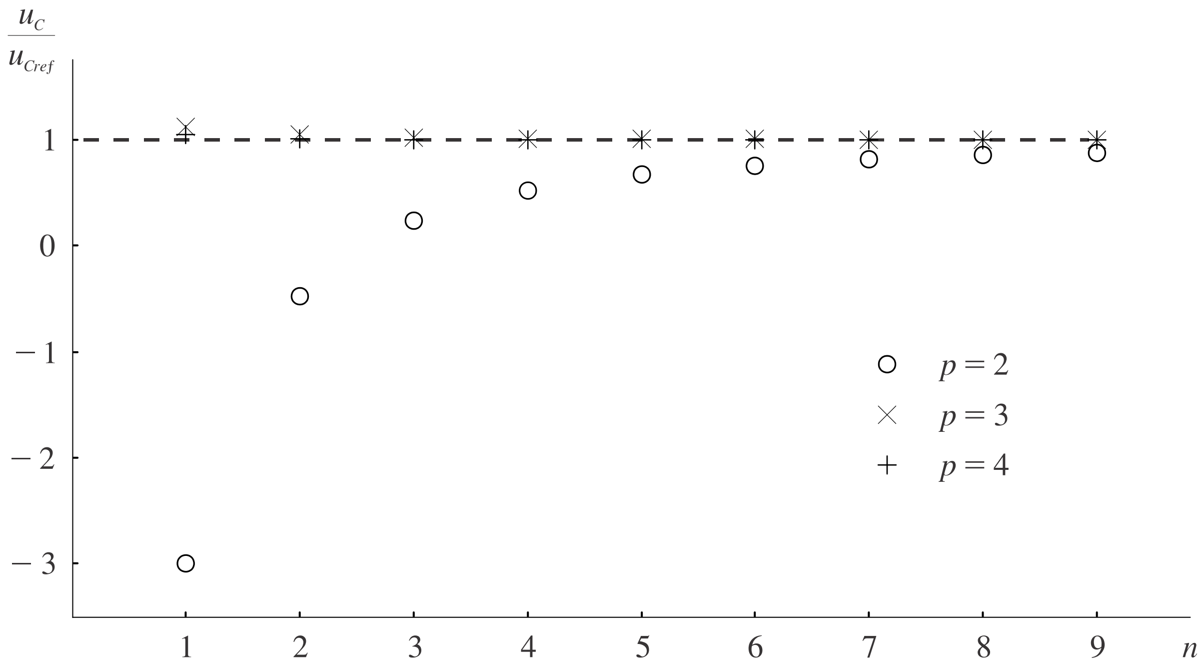

Figure 4: Plate under uniaxial parabolic load: convergence of the u displacement at point *C* under h- and p-refinement

The ratio between our result u_c and $u_{c_{ref}}$ found in Cowper et al. (1970) is plotted against the number n which represents an $n \times n$ mesh. In order to analyze the convergence rate, in Fig. 5 the relative error $\varepsilon_u = |U/U_{ref} - 1|$, where U is the strain energy of the plate and U_{ref} is the benchmark found in Cowper et al. (1970), is plotted against the total number of degrees of freedom using different refinements. The p-refinement is carried out in 1×1 and 3×3 meshes, while the h-refinement is carried out using $p = 2$ and $p = 3$. The advantage of the p-refinement is very clear.

3.2 Centrally cracked plate

A centrally cracked plate, as sketched in Fig. 6, has been chosen to illustrate the performance of the proposed Ritz scheme in the evaluation of the stress intensity factor K. This factor will be obtained by means of

$$K_I{}^2 = -\frac{E}{h}\frac{\partial \Pi}{\partial a} \tag{39}$$

where a is half of the crack length. The derivative $\partial \Pi / \partial a$ is approximated in this paper by central finite difference

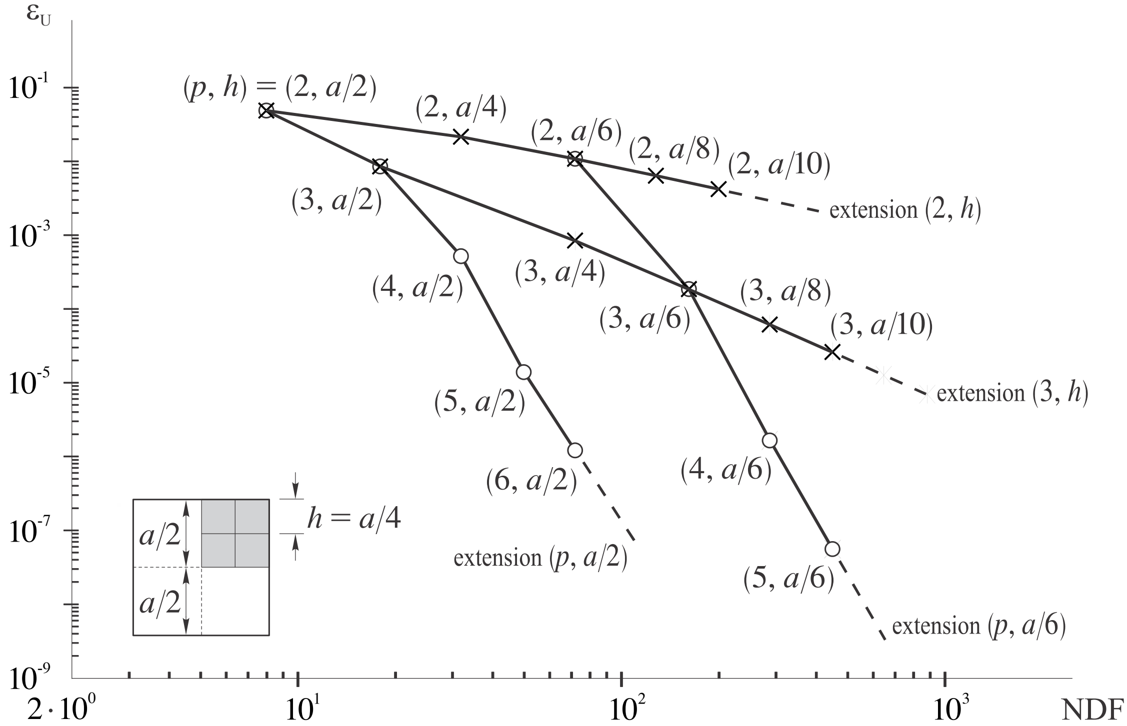

Figure 5: Plate under uniaxial parabolic load: error ε_u against the number of degrees of freedom NDF

$$\frac{\partial \Pi}{\partial a} \approx -\frac{\Pi(a+\Delta a)-\Pi(a-\Delta a)}{2\Delta a} \qquad \Delta a = 0.01a. \tag{40}$$

Our results are presented as the ratio of the stress intensity factor K_I obtained and that of a cracked infinite plate ($L = b = \infty$). They will be denoted by

$$\beta = \frac{K_I}{K_0} \qquad K_0 = q\sqrt{\pi a}/h. \tag{41}$$

The plate has $L = 30$, $b = 10$ and thickness $h = 1$, material properties given by $E = 1$ and $\nu = 0.3$, and is subjected to a uniformly distributed load q (consistent units are used). Due to the double symmetry, only the highlighted quarter of the plate at the right top will be defined as the solution domain and divided into two panels in the y direction: the first panel in the interval $b < y < b + a$ and the second in $b + a < y < 2b$. The geometric boundary conditions

$$u = 0 \quad \text{at} \quad x = L, b + a < y < 2b \qquad v = 0 \quad \text{at} \quad y = b \tag{42}$$

Proceedings of the XXXVIII Iberian Latin-American Congress on Computational Methods in Engineering
P.O. Faria, R.H. Lopez, L.F.F. Miguel, W.J.S. Gomes, M. Noronha (Editores), ABMEC, Florianópolis, SC, Brazil, November 5-8, 2017.

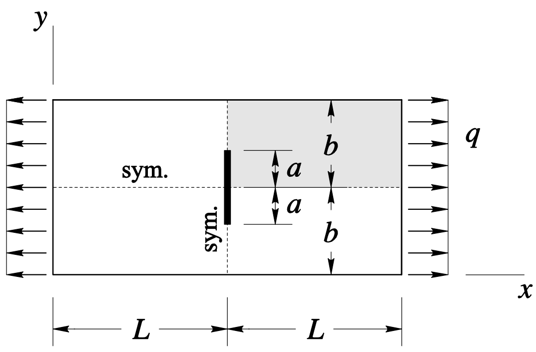

Figure 6: Centrally cracked plate

must be imposed. Table 3 compares our results with those found in Tada (2000). For each crack length it is shown the results for $p = 10, 20, \ldots 50$. There is excellent agreement with the benchmark results, where difference smaller than 1% for $p = 30$ is observed. In order to analyze the convergence rate, in Fig. 7 the relative error $\varepsilon_\beta = |\beta/\beta_{ref} - 1|$ is plotted against the number of degrees of freedom using different refinements for crack length $a/b = 0.5$. The p-refinement is carried out in a two element mesh, while the h-refinement is carried out using $p = 2$ and $p = 5$. The results obtained with meshes of Nastran CQUAD4 (2014) elements are also included in the figure. The advantage of the p-refinement is very clear.

Table 3: Values of β / β_{ref} for a centrally cracked plate

		N				
a/b	β_{ref}	10	20	30	40	50
0.1	1.006	0.932	0.985	0.993	0.996	0.998
0.2	1.024	0.970	0.992	0.997	0.998	0.999
0.3	1.058	0.977	0.994	0.998	0.999	0.999
0.4	1.109	0.979	0.995	0.998	0.999	0.999
0.5	1.186	0.980	0.995	0.998	0.999	1.000
0.6	1.303	0.978	0.995	0.998	0.999	1.000
0.7	1.487	0.974	0.994	0.998	0.999	1.000
0.8	1.814	0.964	0.992	0.997	0.999	1.000

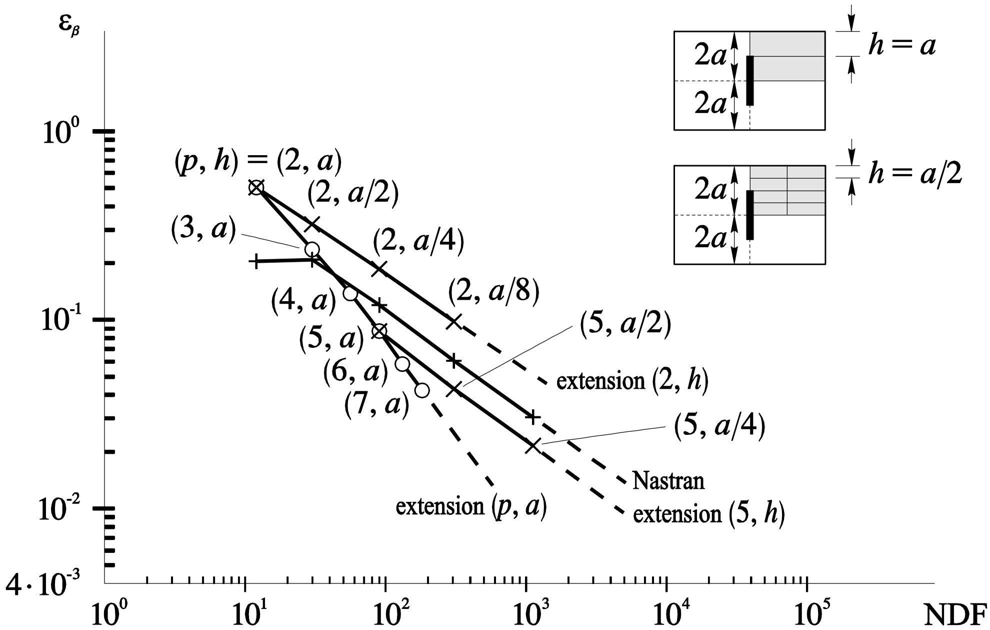

Figure 7: Error $\varepsilon_\beta = |\beta\, /\, (\beta_{ref} - 1)|$ versus number of degrees of freedom for a centrally cracked plate

3.3 Edge cracked plate

The stress intensity factor is evaluated for the plate of Fig. 8. The plate has $L = 15$, $b = 10$ and thickness $h = 1$, material properties given by $E = 1$ and $\nu = 0.3$, and is subjected to a uniformly distributed load q (consistent units are used). Due to the symmetry, only the highlighted half of the plate will be defined as the solution domain and divided into two panels in the y direction: the first panel in the interval $0 < y < a$ and the second in $a < y < b$. The geometric boundary condition

$$u = 0 \qquad \text{at} \qquad x = L, a < y < b \tag{43}$$

must be imposed. Table 4 compares our results with those found in Tada (2000). For each crack length it is shown the results for $p = 10, 20, \ldots 50$. Once again, there is excellent agreement with the benchmark results, where difference smaller than 1% for $p = 30$ is observed.

4 CONCLUSION

This paper introduces a Ritz scheme that can be used to estimate the stress intensity factors for cracked plates. Such a scheme presents a simple and accurate formulation which remains versatile, in the sense that any cracked plate can be solved, as long as all the cracks

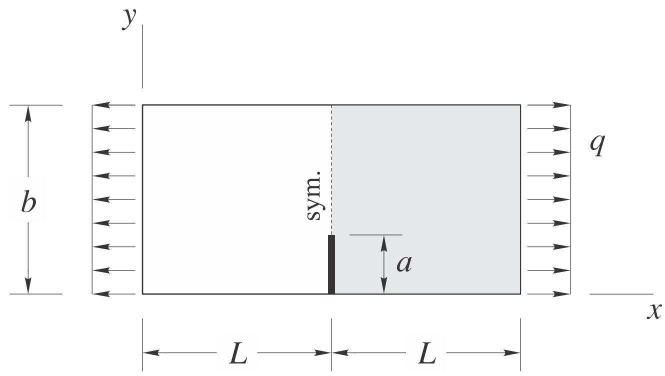

Figure 8: Edge cracked plate

and plate edges are orthogonal. Three different configurations have been analyzed, starting with a square plate under uniaxial parabolic load, that shown us the quality of our model. Then a centrally cracked plate and an edge cracked plate. The results have been compared to both analytical and finite element results. In all the examples we were able to obtain excellent agreement with benchmark solutions. The results can be improved simply by adding more functions, improving the quality of the model as desired. Our proposed structure also shows remarkable efficiency for such accuracy, being extremely precise while still using very little processing power.

Table 4: Values of β / β_{ref} for a centrally cracked plate

		N				
a/b	β_{ref}	10	20	30	40	50
0,1	1,196	0,958	0,986	0,991	0,993	0,993
0,2	1,367	0,976	0,994	0,998	0,999	0,999
0,3	1,655	0,981	0,997	1,000	1,002	1,002
0,4	2,108	0,979	0,996	0,999	1,000	1,001
0,5	2,827	0,975	0,993	0,997	0,998	0,998
0,6	4,043	0,969	0,990	0,994	0,996	0,996
0,7	6,376	0,961	0,988	0,993	0,995	0,995
0,8	11,993	0,946	0,984	0,991	0,994	0,995

REFERENCES

Abadir, K. H., & Magnus, J. R., 2005, *Matrix Algebra*. Cambridge University Press, Cambridge.

Andersson, B., Falk, U., Babuska, I., & von Petersdorff, T., 1995, Reliable stress and fracture mechanics analysis of complex components using a *h-p* version of FEM. *International Journal for Numerical Methods in Engineering*, vol. 38, pp. 2135-2163.

Babuska, I., Griebel, M., & Pitkaranta, J., 1989, The problem of selecting the shape functions for a *p*-type finite element. *International Journal for Numerical Methods in Engineering*, vol. 28, pp. 1891-1908.

Bardell, N. S., 1991, Free vibration analysis of a flat plate using the hierarchical finite element method. *Journal of Sound and Vibration*, vol. 151, pp. 263-289.

Barrette, M., Berry, A., & Beslin, O., 2000, Vibration of stiffened plates using hierarchical trigonometric functions. *Journal of Sound and Vibration*, vol. 235, pp. 727-747.

Basu, P. K., Rossow, M. P., & Szabo, B. A., 1977, *Theoretical Manual and Users' Guide for COMET-X*. Technical Report FRA/ORD-77/60, Washington University.

Beslin, O., & Nicolas, J., 1996, A hierarchical functions set for predicting very high order plate bending modes with any boundary conditions. *Journal of Sound and Vibration*, vol. 202, pp. 633-655.

Brighenti, R., 2005, Numerical buckling analysis of compressed or tensioned cracked thin plates. *Engineering Structures*, vol. 27, pp. 265-276.

Cowper, G. R., Lindberg, G. M., & Olson, M. D., 1970, A Shallow Shell Finite Element of Triangular Shape. *International Journal of Solids and Structures*, vol. 6, pp. 1113-1156.

Fawaz, S. A., & Andersson, B., 2004, Accurate stress intensity factor solutions for corner cracks at a hole. *Engineering Fracture Mechanics*, vol. 71, pp. 1235-1254.

Isida, M., Tagami, S., & Itagaki, Y., 1962, Stress concentration due to a central transverse crack in a strip reinforced on either sides. *The Journal of the Japan Society of Aeronautical Engineering*, vol. 10, pp. 141-149 (in Japanese).

Kumar, S., & Paik, J. K., 2004, Buckling analysis of cracked plates using hierarchical trigonometric functions. *Thin-Walled Structures*, vol. 42, pp. 687-700.

NX Nastran, 2014. *Element Library Reference*, Siemens PLM Software.

Poe Jr, C. C., 1971, *The Stress intensity factor calculated for cracked sheet with riveted and uniformly spaced stringers*. Technical Report NASA TR R-358, Langley Research Center.

Rooke, D. P., & Cartwright D. J., 1976, *Compendium of Stress Intensity Factors*. HMSO, London.

Tada, H., Paris, P. C., & Irwin, G. R., 2000. *The Stress Analysis of Cracks Handbook*, 3rd ed., ASME Press, New York.

Zhu, D. C., 1986, Development of hierarchical finite element methods at BIAA, vol. 1. In *Proceedings of the International Conference on Computational Mechanics*, Tokyo, Japan.